*molecules*

MDPI

*Article*

# Designed Syntheses of Three {$Ni_6PW_9$}-Based Polyoxometalates, from Isolated Cluster to Cluster-Organic Helical Chain

**Chong-An Chen, Yan Liu and Guo-Yu Yang ***

MOE Key Laboratory of Cluster Science, School of Chemistry and Chemical Engineering, Beijing Institute of Technology, Beijing 102488, China; cca@bit.edu.cn (C.-A.C.); liuyanik@163.com (Y.L.)
* Correspondence: ygy@bit.edu.cn or ygy@fjirsm.ac.cn

**Abstract:** Three new hexa-Ni-substituted Keggin-type polyoxometalates (POMs), $[Ni_6(OH)_3(DACH)_3(H_2O)_6(PW_9O_{34})]\cdot 31H_2O$ (**1**), $[Ni(DACH)_2][Ni_6(OH)_3(DACH)_3(HMIP)_2(H_2O)_2(PW_9O_{34})]\cdot 56\ H_2O$ (**2**), and $[Ni(DACH)_2][Ni_6(OH)_3(DACH)_2(AP)(H_2O)_5(PW_9O_{34})]\cdot 2H_2O$ (**3**) (DACH = 1,2-Diami- nocyclohexane, MIP = 5-Methylisophthalate, AP = Adipate) were successfully made in the presence of DACH under hydrothermal conditions. **1** is an isolated hexa-Ni-substituted Keggin unit decorated by DACH. In order to further construct POM cluster-organic frameworks (POMCOFs) on the basis of **1**, by analyzing the steric hindrances and orientations of the POM units, the rigid HMIP and flexible AP ligands were successively incorporated, and another anionic monomeric POM **2** and the new 1D POM cluster organic chain (POMCOC) **3** were obtained. HMIP ligand still acts as a decorating group on the $Ni_6$ core of **2** but results in the different spatial arrangement of the {$Ni_6PW_9$} units. AP ligands in **3** successfully bridge adjacent isolated POM cluster units to 1D POMCOC with left-hand helices. The AP in **3** is the longest aliphatic carboxylic acid ligand in POMs, and the 1D POM cluster-AP helical chain represents the first 1D POMCOC with a helical feature.

**Keywords:** polyoxometalates; hydrothermal syntheses; cluster-organic frameworks; helical chain



**Citation:** Chen, C.-A.; Liu, Y.; Yang, G.-Y. Designed Syntheses of Three {$Ni_6PW_9$}-Based Polyoxometalates, from Isolated Cluster to Cluster-Organic Helical Chain. *Molecules* **2022**, *27*, 4295. https://doi.org/10.3390/molecules27134295

Academic Editor: Xiaobing Cui

Received: 25 May 2022
Accepted: 2 July 2022
Published: 4 July 2022



## 1. Introduction

In the past century, polyoxometalates (POMs) have been widely researched for their abundant structures and applications in catalytic [1–3], magnetic [4], and electrical fields [5,6]. In order to enrich POMs' structural chemistry and further expand or optimize their applications, researchers have started to design and construct POM cluster organic frameworks (POMCOFs) [7–9] which is a new and promising branch of cluster organic frameworks (COFs) [10–12]. Since the POMCOF was reported [13], considerable efforts have been made in building POMCOFs with Keggin-/Anderson-/Lindqvist-POM secondary building units (SBUs) and rigid aromatic organic linkers [7,8,14,15]. However, compared with the traditional MOFs, the designed syntheses of POMCOFs are still facing huge challenges for the following two reasons: (1) POM clusters have large negative charges and oxygen-rich surfaces, which facilitate their bonding to metal cations, rather than the O-/N-donors from organic linkers. (2) POMs are rigid and stable clusters, therefore, the steric hindrance effects of POM SBUs and linkers need to be well-matched during assembly. Hence, how to choose proper POM SBUs and organic linkers is the key to constructing POMCOFs.

Among seven typical types of POMs, only Anderson-/Lindqvist-/Keggin-types have been successfully applied as SBUs in POMCOFs. Since 2016, the first Anderson-type POM-based heterometallic cluster organic framework was made; Anderson-type POMs have become the popular choice for SBUs [8]. The combination of Anderson-type SBU and rigid bifunctional tris(alkoxo) ligand with a pyridyl group opens up the gate of Anderson-type POMCOFs' world. Lindqvist-type POMs are important members of the POMs family. Though five different elements can all produce the Lindqvist-type $[M_6O_{19}]^{n-}$ (M = $V^V$, $Nb^V$, $Ta^V$, $Mo^{VI}$, $W^{VI}$) cluster, only polyoxovanadates have been successfully applied as

SBUs in Lindqvist-type POMCOFs [15,16]. So far, most of the reported POMCOFs are made with Keggin-type POM SBUs [7,13,14,17–20]. In these POMCOFs, most of the SBUs are saturated {ε-$M_4PMo_{12}O_{40}$} (M=La, Zn) [13,14,17–19], of which, the incorporation of M (M=$Zn^{2+}$, $La^{3+}$) provide the easier bonding sites than the saturated {$PMo_{12}$} units for organic linkers. Our group has long been devoted to transition metal substituted POMs (TMSPs) based on the trilacunary Keggin fragments under hydrothermal conditions. From our perspective, the trilacunary sites of the [$XW_9O_{34}$] (P, W, Ge) unit can act as structure-directing agents (SDAs) to induce transition metal ions' aggregation to cluster, on which the terminal end of water molecules may facilitate the substitutions of organic linkers in constructing Keggin-type POMCOFs. Since the first hexa-$Ni^{II}$ substituted TMSP based on trilacunary Keggin fragments was made [4], we have been working on POMs structural chemistry based on hexa-$Ni^{II}$-substituted POMs and have already mastered the synthetic conditions of hexa-$Ni^{II}$ substituted Keggin POMs. By using {$Ni_6PW_9$} SBUs and rigid aromatic carboxylate ligands, we have built a series of novel Keggin-type POMCOFs [7,20]. Hence, we believe that some other intriguing POMCOFs can be made by using {$Ni_6PW_9$} SBUs with proper organic linkers.

Rigid and semi-rigid aromatic carboxylate ligands are the common linkers being used in making POMCOFs [7,20–22]; their rigid structures are favorable for the stabilization of the frameworks. However, the large steric hindrance effects of POMs and rigid ligands sometimes cannot match to form POMCOFs. To overcome this difficulty, alipha- tic dicarboxylic acid may be a potential candidate due to its smaller steric hindrances and better flexibilities, which may produce some intriguing frameworks with helical or interpenetrating features that cannot be obtained with rigid aromatic ligands. However, little relevant research has been made, including two typical examples containing aliphatic dicarboxylic acid-bridges for a 2D POMCOF and a tetramer [23,24]. Hence, in this work, we first made an isolated hexa-Ni-substituted Keggin-type POM [$Ni_6(OH)_3$-$(DACH)_3(H_2O)_6(PW_9O_{34})$]·$31H_2O$ (**1**) under hydrothermal conditions. The abundant terminal water molecules on the $Ni_6$ cores are potential substitution sites for organic linkers, which help us to further construct POMCOFs. When we first applied the rigid carboxylate ligand MIP, another hexa-Ni-substituted Keggin-type monomer [$Ni(DACH)_2$]-[$Ni_6(OH)_3(DACH)_3(HMIP)_2$-$(H_2O)_2(PW_9O_{34})$]·$56H_2O$ (**2**) was obtained, HMIP ligands still decorate on the $Ni_6$ cores, failing to bridge the POM clusters. By analyzing the structure of **2**, we used the aliphatic dicarboxylate AP ligands as a linker and a new 1D POMCOC with helical chains [$Ni(DACH)_2$][$Ni_6(OH)_3(DACH)_2(AP)(H_2O)_5(PW_9O_{34})$]·$2H_2O$ (**3**) was made. To the best of our knowledge, the AP in **3** is the longest aliphatic dicarboxylic acid being incorporated in POMs. Moreover, the 1D helical chain of **3** is the first 1D POMCOC with helical features.

## 2. Experimental Section

### *2.1. General Procedure*

All the reagents were analytical grade and used without any further purification. $Na_{10}$[A-α-$PW_9O_{34}$]·$7H_2O$ was prepared by a method from the literature [25]. Meso-form DACH was used in the syntheses. The powder X-Ray diffraction (PXRD) patterns of the three compounds were collected on a Bruker D8 Advance X-ray diffractometer (Bruker, Karlsruhe, Germany) with Cu Kα radiation (λ = 1.54056 Å) and 2θ scanning from 5–50°. UV-Vis absorption spectra were obtained on a Shimadzu UV3600 spectrometer (Shimadzu, Kyoto, Japan) with wavelengths from 190 to 800 nm. IR spectra were recorded on a Nicolet iS10 FT-IR spectrometer (Thermo Fisher Scientific, Waltham, MA, USA) with the wavenumbers ranging from 4000 to 400 $cm^{-1}$. Thermogravimetric analyses were conducted on a Mettler Toledo TGA/DSC 1100 analyzer (Mettler Toledo, Zurich, Switzerland) heating up from 25–1000 °C (heating rate: 10 °C/h) under an air atmosphere. Elemental analyses proceeded on the EuroEA3000 elemental analyzer (EuroVector, Pavia, Italy).

### *2.2. Syntheses*

#### 2.2.1. Synthesis of **1**

$Na_9[A\text{-}\alpha\text{-}PW_9O_{34}]\cdot 7H_2O$ (0.320 g, 0.125 mmol) and $NiCl_2\cdot 6H_2O$ (0.820 g, 3.44 mmol) were stirred in 9 mL 0.5 mol/L sodium acetate buffer (pH = 4.8) for 10 min; then, 3 mL DACH (Scheme 1a) was slowly dropped in and continually stirred for 30 min. The resulting solution was sealed in a 25 mL Teflon-lined stainless-steel autoclave and heated at 170 °C for 5 days. After cooling down to room temperature and washing with distilled water, green rod-like crystals were obtained with a yield of 34% (based on $Na_9[A\text{-}\alpha\text{-}PW_9O_{34}]\cdot 7H_2O$). Elemental analysis calcd (%): C, 5.93; H, 3.26; and N, 2.30 (based on $[Ni_6(OH)_3(DACH)_3(H_2O)_6(PW_9O_{34})]$ -·$31H_2O$). Found: C, 7.10; H, 2.17; N, 2.81. IR(KBr, $cm^{-1}$): 3428(s), 3332(w), 3280(w), 2929(w), 2856(w), 1628(w), 1588(w), 1449(w), 1377(w), 1231(w), 1119(w), 1039(s), 941(vs), 842(vs), 796(vs), and 716(vs).

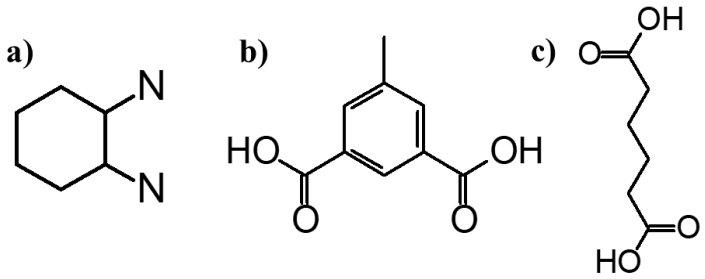


**Scheme 1.** DACH (**a**), MIPA (**b**), and AA (**c**) ligands in **1**–**3**.

#### 2.2.2. Syntheses of **2** and **3**

The synthetic procedures of **2** and **3** were the same as **1,** except for the adding of MIPA (5-Methylisophthalic Acid, Scheme 1b) (0.200 g, 1.11 mol) and AA (Adipic Acid, Scheme 1c) ligands (0.200 g, 1.37 mol) for **2** and **3**, with the yield of 36% and 28%, respectively. Based on $Na_9[A\text{-}\alpha\text{-}PW_9O_{34}]\cdot 7H_2O$. Elemental analysis calcd (%) for **2**: C, 12.34; H, 4.35; and N, 3.00 (based on $[Ni(DACH)_2][Ni_6(OH)_3(DACH)_3(HMIP)_2(H_2O)_2(PW_9O_{34})]$·- 56 $H_2O$). Found: C, 14.10; H, 3.37; N, 3.39. IR(KBr, $cm^{-1}$): 3458(s), 3338(w), 3264(w), 2929(w), 2859(w), 1562(w), 1361(w), 1033(w), 935(vs), 841(vs), 796(vs), and 715(vs). Elemental analysis calcd (%) for **3**: C, 10.53; H, 2.36; and N, 3.27 (based on $[Ni(DACH)_2][Ni_6(OH)_3(DACH)_2(AP)(H_2O)_5(PW_9O_{34})]\cdot 2H_2O$). Found: C, 10.44; H, 2.63; and N, 3.34. IR(KBr, $cm^{-1}$): 3423(s), 3240(w), 2923(w), 2860(w), 1591(w), 1546(w), 1413(w), 1037(s), 943(vs), 848(vs), 796(vs), and 710(vs).

### *2.3. X-ray Crystallography*

The single-crystal diffraction data of **1**–**3** were collected on a Gemini A Ultra CCD diffractometer with graphite monochromated Mo Kα (Λ = 0.71073 Å) radiation at 296(2) K. The structures were solved by direct methods and refined by the full-matrix least-squares fitting on $F^2$ method with the SHELX-2008 program package [26]. Anisotropic displacement parameters were refined for all atomic sites except for some disordered atoms. The contribution of the disordered solvent molecules in **1** and **2** was treated with the SQUEEZE method in PLATON (Utrecht University, Utrecht, The Netherlands). In the refinements, 0, 1, and 2 lattice water molecules were found for **1**–**3** from the Fourier maps, respectively. Based on the potential solvent-accessible voids and electron counts from the SQUEEZE reports, there were 31 and 55 lattice water molecules removed for **1** and **2**, respectively. According to the elemental analyses and TGA, there are 27 and 34 lattice water molecules lost from efflorescence in **1** and **2**, respectively. In **3**, 4 absorbed water molecules were found. Basic crystallographic data and structural refinement data are listed in Table 1. Detailed crystallographic data have been deposited on the Cambridge Crystallographic Data Centre: CCDC 2171028 (for **1**), 2170965 (for **2**), and 2170966 (for **3**). These data can be obtained free of charge via http://www.ccdc.cam.ac.uk/conts/retrieving.html accessed on 29 June 2022

or from the Cambridge Crystallographic Data Centre, 12 Union Road, Cambridge CB2 1EZ, UK; Fax: +44-1223-336-033; or email: deposit@ccdc.cam.ac.uk.

**Table 1.** Crystallographic data and structural refinements for **1**–**3**.

| | **1** | **2** | **3** |
|---|---|---|---|
| Formula | $Ni_6PW_9O_{74}C_{18}H_{119}N_6$ | $Ni_7PW_9O_{103}C_{48}H_{203}N_{10}$ | $Ni_7PW_9O_{48}C_{30}H_{81}N_8$ |
| Molecular weight | 3642.06 | 4665.78 | 3418.61 |
| Crystal system | Trigonal | Monoclinic | Orthorhombic |
| Space group | *P*-3*c*1 | $P2_1/c$ | $P2_12_12_1$ |
| *a*/Å | 18.1775 | 24.9850 | 36.6105 |
| *b*/Å | 18.1775 | 14.9500 | 14.1605 |
| *c*/Å | 21.3261 | 26.6410 | 13.8492 |
| *α*/° | 90 | 90 | 90 |
| *β*/° | 90 | 98.697 | 90 |
| *γ*/° | 120 | 90 | 90 |
| *V*/Å$^3$ | 6102.5 | 9837 | 7179.7 |
| *Z* | 4 | 4 | 4 |
| *Dc*/g cm$^{-3}$ | 3.964 | 3.151 | 3.163 |
| *μ*/mm$^{-1}$ | 18.880 | 11.956 | 16.263 |
| *F*(000) | 6840 | 9048 | 6312 |
| Goodness-of-fit on $F^2$ | 1.075 | 1.099 | 1.131 |
| *R* indices [$I > 2\sigma(I)$] [1] | 0.0355 (0.0946) | 0.0633 (0.1624) | 0.0601 (0.1350) |
| *R* indices (all data) | 0.0504 (0.1043) | 0.0996 (0.1777) | 0.0704 (0.1413) |

[1] $R_1 = \Sigma||F_0| - |F_c||/\Sigma|F_0|$. $wR_2 = \{\Sigma w[(F_0)^2 - (F_c)^2]^2/\Sigma w[(F_0)^2]^2\}^{1/2}$.

## 3. Result and Discussion

### *3.1. Structure of **1** and Designed Syntheses for **2***

X-ray diffraction analyses reveal that **1** crystallizes in the trigonal space group *P*-3*c*1, consisting of the neutral $[Ni_6(\mu_3\text{-}OH)_3(DACH)_3(H_2O)_6(PW_9O_{34})]$ (**1a**, Figure 1a) cluster. **1a** can be seen as the classical trilacunary Keggin $[B\text{-}\alpha\text{-}PW_9O_{34}]^{9-}$ fragment being capped by a triangular $[Ni_6(\mu_3\text{-}OH)_3]^{9+}$ cluster. Due to the trigonal $C_3$ symmetry of **1**, there are only two independent $Ni^{2+}$ in the $Ni_6$ cluster (Figure S1, Supplementary Materials). Each Ni1 and Ni2 interconnect with each other by edge-sharing, producing three edge-sharing $\{Ni_3O_4\}$ truncated cubanes. Three $Ni1O_6$ octahedra locate on the three lacunary sites of the $\{PW_9\}$ unit, while three $Ni2O_4N_2$ octahedra are on the three vertexes of the triangular $Ni_6$ cluster, further decorated by three DACH ligands, respectively (Figure 1b). According to BVS calculations [27], the bond valance of $\mu_3$-O4 is 1.12, indicating its protonation. **1a** exhibits two opposite orientations, which are alternately arranged with a shoulder-to-shoulder arrangement along the *a*-axis and [110] direction (Figure 1c,d). Such arrangements construct the snowflake-like supramolecular channels with $S_6$ symmetry and are the hydrophobic voids as well (Figure 1e).

The presence of six terminal water molecules on the $Ni_6$ cluster provides abundant substituted sites for organic ligands. We started to incorporate organic ligands into the reaction system of **1**, attempting to construct POMCOFs with proper organic linkers. In our previous work, we have successfully made two 1D POMCOCs $\{[Ni_6(OH)_3(H_2O)_2\text{-}(enMe)_3(PW_9O_{34})](1,3\text{-bdc})\}[Ni(enMe)_2]\cdot 4H_2O$ (**4,** enMe = 1,2-diaminopropane, 1,3-bdc = 1,3-benzenedicarboxylate acid) and $\{[Ni_6(OH)_3(H_2O)(en)_4(PW_9O_{34})](Htda)\}\cdot H_3O\cdot 4H_2O$ (**5,** en = ethylenediamine, tda = thiodiglycolic acid) based on $\{Ni_6PW_9\}$ SBUs and V-type rigid dicarboxylate ligands (1,3-bdc and tda) [7]. To analyze these structures carefully, we found that in **4** and **5**, $\{Ni_6PW_9\}$ SBUs are arranged in shoulder-to-shoulder and face-to-face modes, respectively, which are further bridged by the V-type dicarboxylate ligands to 1D POMCOCs. In **1**, though the opposite-orientated $\{Ni_6PW_9\}$ units exhibit shoulder-to-shoulder arrangements along the *a*-axis, the interunit distances are too close to accommodate the organic ligands. Hence, we choose the similar V-type ligand MIP to see if the methyl group can further spread out the opposite orientated POM units and if the carboxyl groups can bridge adjacent same orientated units to 1D chains at the same time. By adding MIPA into the reaction of **1**, **2** was obtained. The observation of **2** confirms part of our speculations; though HMIP

still acts as a decoration group, it changes the orientations of adjacent POM units such that two different orientated units both arrange in shoulder-to-shoulder modes separately with moderate interunit distances.

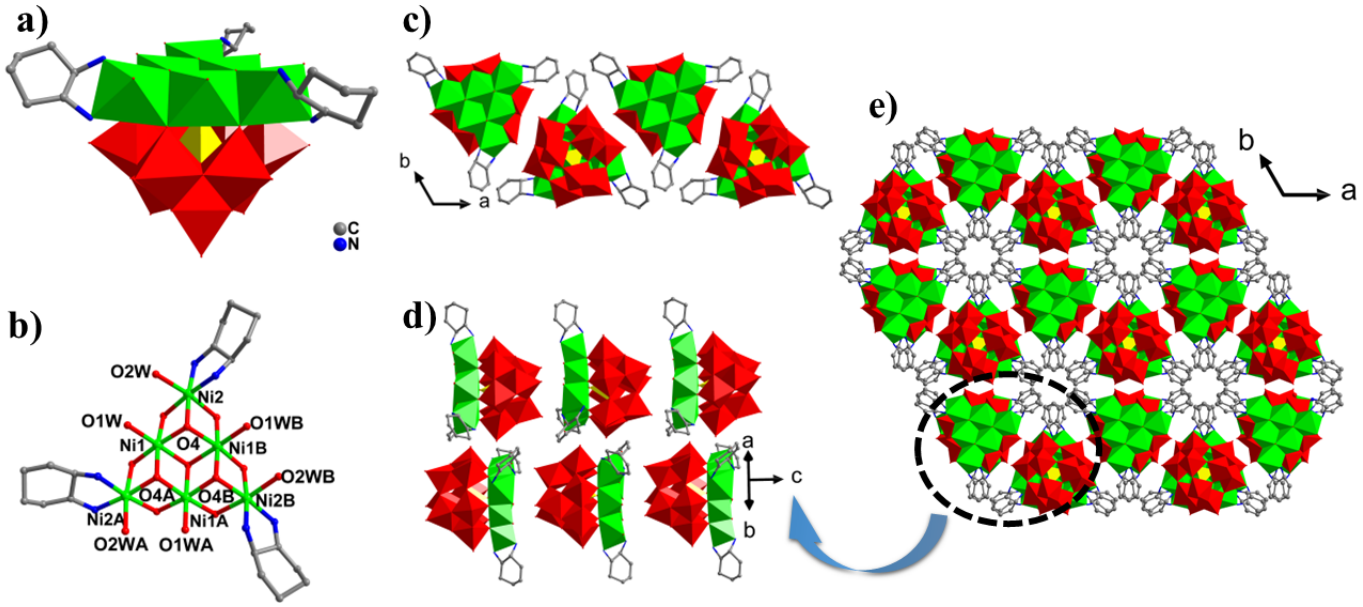


**Figure 1.** (**a**) A polyhedral view of polyoxoanion **1a**.; (**b**) View of the $Ni_6$ cluster in **1a**; (**c**,**d**) Shoulder-to-shoulder arrangements of **1a** with opposite orientations along the *a*-axis and [110] direction; and (**e**) The 3D supramolecular framework of **1**. Color code of polyhedral: $WO_6$: red; $NiO_6/NiO_4N_2$: green; and $PO_4$: yellow. Hydrogen atoms of the ligands are not shown for better clarity.

### *3.2. Structure of* **2** *and Designed Syntheses for* **3**

X-ray diffraction analyses reveal that **2** crystalizes in its monoclinic space group $P2_1/c$. Its polyoxoanionic cluster $[Ni_6(OH)_3(DACH)_3(HMIP)_2(H_2O)_2(PW_9O_{34})]$ (**2a**) is similar to that of **1a**, except for four water molecules in **1a** being replaced by two HMIP ligands in **2a** (Figure 2a,b and Figure S1). This difference makes **2a** an anionic cluster, accompanied by the charge-balancing $[Ni(DACH)_2]^{2+}$ complex, in which $Ni^{2+}$ exhibit the planar square coordination geometry (Figure S2, Supplementary Materials).

Due to the large steric hindrance of HMIP, adjacent opposite-orientated POM clusters are spread out and adopt face-to-face arrangements with each other, while the same orientated units still maintain shoulder-to-shoulder arrangements (Figure 2c,d), which are ideal arrangements for making POMCOFs based on our previous research [7,20]. Using another organic linker with a longer length may help to achieve our aims, but the longer length corresponds to the larger steric hindrances, which may affect the orientations of POM units or increase the interunit distances. Rigid aromatic carboxylic ligands seem unlikely to satisfy our design. Hence, we transfer our focus to chainlike aliphatic dicarboxylic acids. Their higher flexibilities may facilitate their bridging functions on POM SBUs with more flexible orientations and interunit distances and may further result in some intriguing interpenetrating or helical structures that cannot be obtained with rigid aromatic carboxyl ligands. We found that the bilateral DACH molecules on each $Ni_6$ cluster prevent the bridging of adjacent same-orientated SBUs with organic linkers (Figure 2d,e). Additionally, the distance between two terminal –COOH groups from adjacent opposite-orientated POM SBUs is 6.20 Å (Figure 2e), which is nearly matchable with that of AP in the reported polymers (6.30 Å, Figure 2f) [28]. Using AP to replace HMIP ligand in **2** may achieve our goals. Based on the above considerations, AP was used as a linker in the synthesis of **3**. Under similar synthetic conditions with **1** and **2**, **3** was obtained. AP ligand successfully bridges adjacent opposite orientated POM cluster units to the unpreceded 1D helical chains.

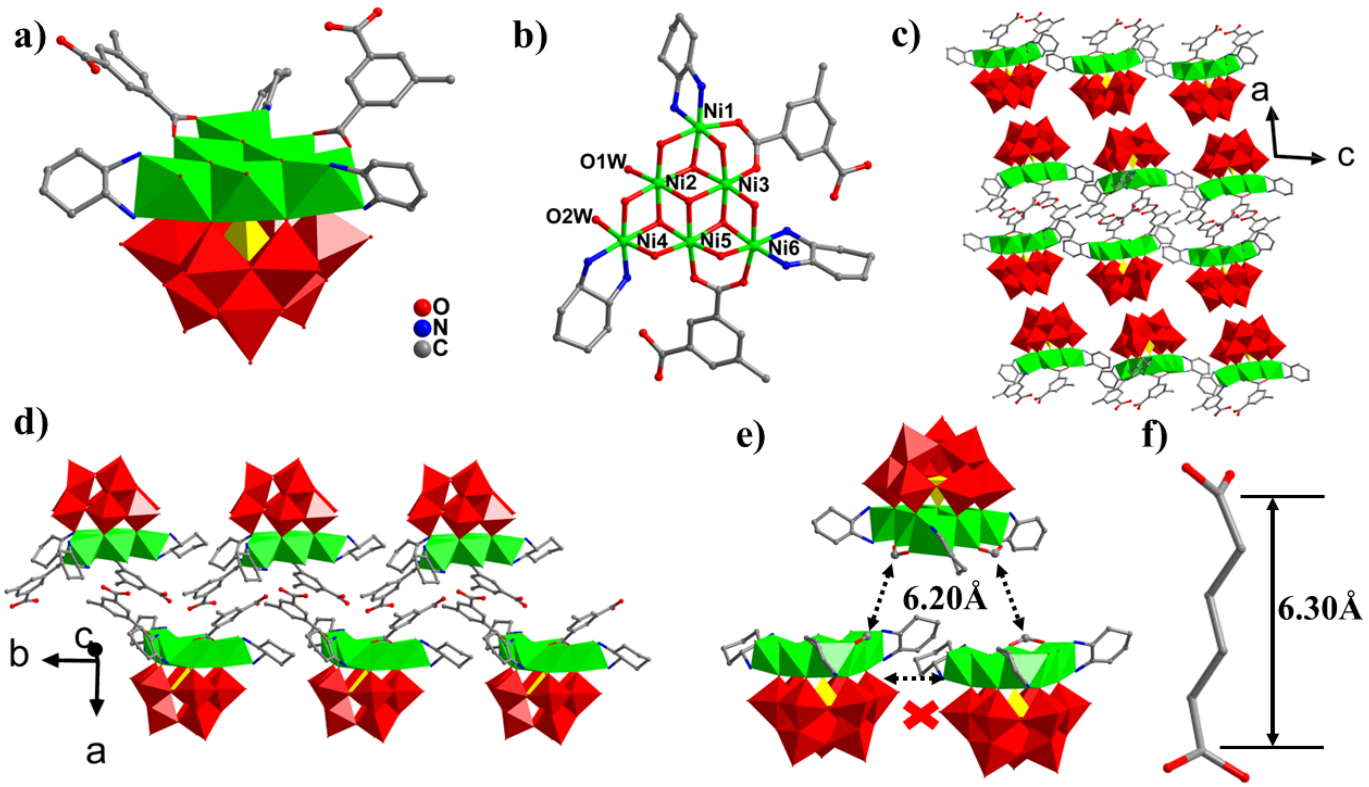


**Figure 2.** (**a**) A polyhedral view of polyoxoanion **2a**.; (**b**) View of the $Ni_6$ cluster in **2a**; (**c**) Spatial arrangements of **2a** along with the *a*-and *c*- axes; (**d**) Spatial arrangements of **2a** along the *b*-axis; (**e**) Interunit distances of **2a**; and (**f**) Matchable distance of AP ligand. Color code of polyhedral: $WO_6$: red; $NiO_6$/$NiO_4N_2$: green; and $PO_4$: yellow. Hydrogen atoms of the ligands are not shown for better clarity.

### *3.3. Structure of* ***3***

**3** crystallizes in the orthorhombic space group $P2_12_12_1$. Its asymmetric unit contains a $[Ni_6(OH)_3(DACH)_2(AP)(H_2O)_5(PW_9O_{34})]$ (**3a**) cluster (Figure 3a), a $[Ni(DACH)_2]^{2+}$ complex, and two lattice water molecules (Figure S1, Supplementary Materials). Compared with **1a** and **2a**, only four-terminal water molecules are substituted by two bidentate DACH ligands on the $Ni_6$ cluster of **3a** (Figure 3b). Each $Ni_6$ cluster links with two AP, of which, one terminal carboxyl group of the AP replaces two terminal water molecules on Ni5 and Ni6, while another carboxyl group replaces only one water molecule on Ni1 (Figure 3b). Each AP ligand bridges two $Ni_6$ clusters (Figure 3c). Such substitution and linkage successfully construct the 1D helical chain with left-hand helices around a $2_1$-screw axis (Figure 3d,e). Adjacent 1D chains stack in -ABAB- and -AAA- sequences along the *a*-and *c*-axis, respectively (Figure 3f,g). It is worth noting that the orientation of each POM SBU and interunit distance have been continually adjusted to the face-to-shoulder arrangements with shorter interunit distance to match the linkage of AP ligand, which are different from those in rigid dicarboxylate ligand-bridged POMCOFs. Such special arrangements of POM SBUs, and the good flexibility of AP, synergistically contribute to the 1D helical chains with left-hand helices. Similar to that in **2**, $[Ni(DACH)_2]^{2+}$ complexes with planar square configuration locate interchain to compensate for the negative charges of the chains (Figure S2, Supplementary Materials).

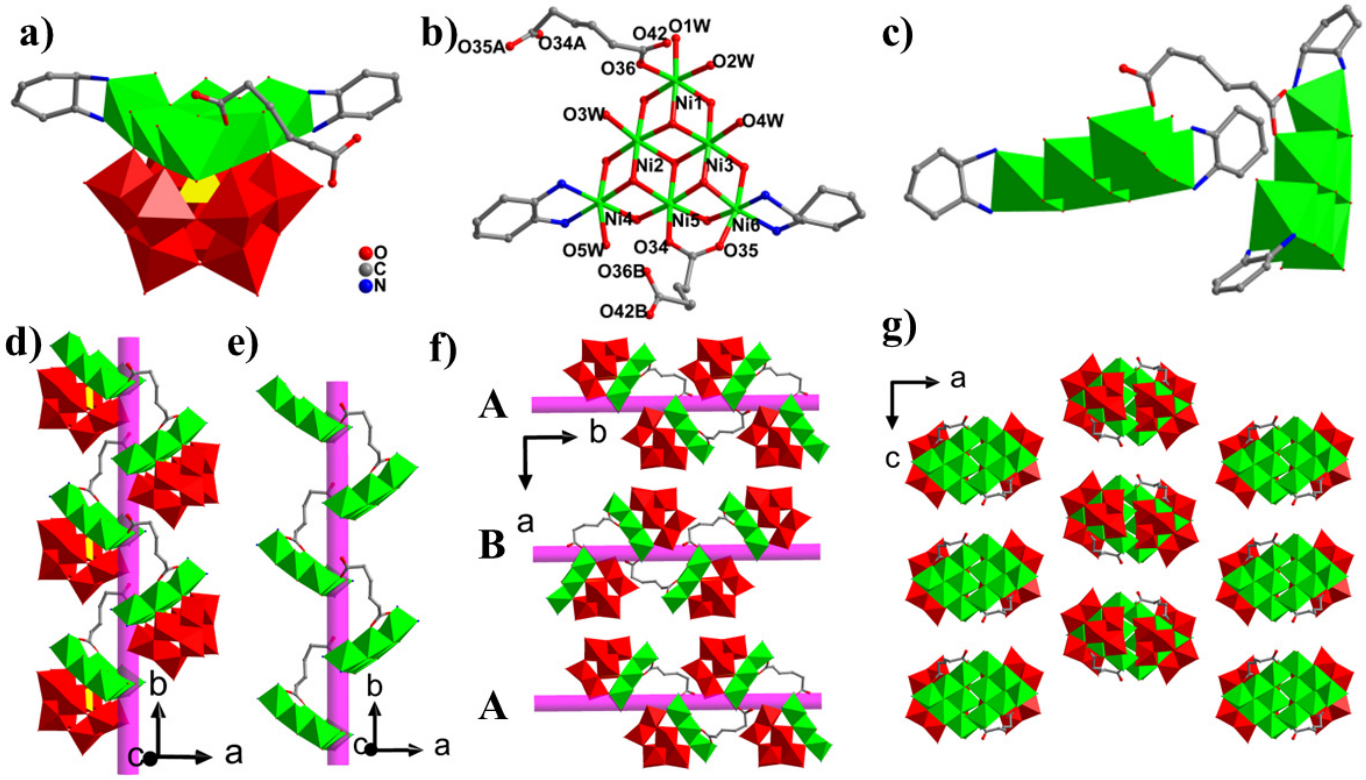


**Figure 3.** (**a**) A polyhedral view of polyoxoanion **3a**.; (**b**) View of the $Ni_6$ cluster and its' linkage with AP; (**c**) The linkage of AP with adjacent $Ni_6$ cluster; (**d**) View of the 1D helical chains with left-hand helices along the *b*-axis; (**e**) The simplified sketch of the $Ni_6$-AP 1D chain; and (**f**,**g**) The -ABAB- and -AAA- stacking modes along *a*-and and *c*-axis, respectively. Color code of polyhedral: $WO_6$: red; $NiO_6/NiO_4N_2$: green; and $PO_4$: yellow. Hydrogen atoms of the ligands are not shown for better clarity.

### *3.4. Structural Comparisons*

In TMSPs' abundant structural chemistry, POM clusters have various linkages with each other to generate different 1D/2D/3D structures:

First, the interconnections of POM clusters (including different structural types) and rigid aromatic organic ligands. This linkage produces most of the 3D POMCOFs, while 1D chains and 2D layers are relatively rare through this connection, except for these three examples: the 1D chains built from the $\{Ni_6PW_9\}$ unit and 1,3-bdc, tda ligand (Figure 4a,b) [7], respectively, and the layer made by another ethylenediamine-func- tionalized $\{Ni_6PW_9\}$ unit and 1,3-bdc ligand (Figure 4c) [20].

Second, the interconnections of TMSP cluster units through TM-O=W bonds. This linkage generates a series of 1D chains and 2D layers [29,30]. The 3D open frameworks constructed by the pure TM–O=W linkage are only observed in $Cu^{II}$-substituted TMSPs, including $[\{Cu_6(\mu_3\text{-}OH)_3(en)_3(H_2O)_3\}(B\text{-}\alpha\text{-}PW_9O_{34})]\cdot 7H_2O$ and $[Cu_6(\mu_3\text{-}OH)_3(en)_3(H_2O)_3(B\text{-}\alpha\text{-}PW_9O_{34})]\cdot 4H_2O$ (Figure 4d), which are caused by the unique Jahn–Teller effect of $CuO_4N_2$ octahedra with the axial elongation [31,32].

Third, the TMSP frameworks with TM complex-bridges. TM complex-bridges are common in TMSPs' frameworks. They can extend the POM units to 1D/2D/3D frameworks through TM–O=W, TM–O–TM, and TM–N···N-TM linkages [33–36].

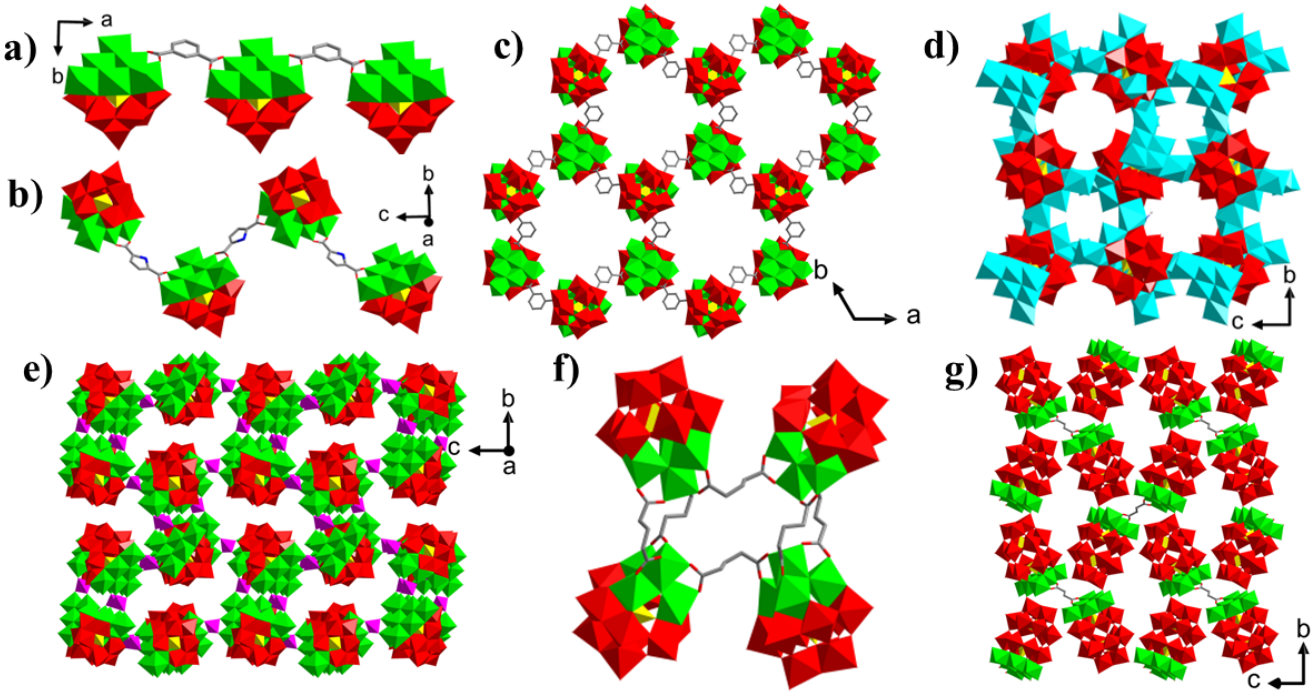


**Figure 4.** (**a**) One-dimensional chain built from $\{Ni_6PW_9\}$ unit and 1,3-bdc ligand; (**b**) One- dimensional chain built from $\{Ni_6PW_9\}$ unit and tda ligand; (**c**) Two-dimensional layer built from $\{Ni_6PW_9\}$ unit and 1,3-bdc ligand; (**d**) Three-dimensional framework built from the interconnection of $\{Cu_6PW_9\}$ unit through Cu–O=W linkage; (**e**) Three-dimensional framework built from $\{Ni_6PW_9\}$ unit and $WO_4$ tetrahedron; (**f**) Tetramer built from $\{Ni_4SiW_9\}$ and glutaric acid linker; and (**g**) Two-dimensional layer built from Dawson-type $\{Ni_6P_2W_{15}\}$ unit and succinic acid linker. Color code of polyhedral: $WO_6$: red; $NiO_6/NiO_4N_2$: green; $PO_4$: yellow; $CuO_6$: light blue; and $WO_4$: purple. Hydrogen atoms of the ligands are not shown for better clarity.

Fourth, is the TMSP framework with $WO_4$ bridges. However, to the best of our knowledge, it was only found in the first chiral 3D framework of $[Ni(enMe)_2]_3[WO_4]_3$-$[Ni_6(enMe)_3(OH)_3PW_9O_{34}]_2{\cdot}9H_2O$ (Figure 4e) [37].

Compared with these TMSP-based frameworks with four different linkages, the 1D helical chains in **3** represent a new structural type of POMCOCs. Aliphatic dicarboxylic acid ligands are rare not only in POMCOFs but also in POMs. Limited evidence includes the glutaric acid-bridged tetramer $[\{(SiW_9O_{34})Ni_4(OH)_3\}_4(OOC(CH_2)_3COO)_6]$ (Figure 4f) and the succinic acid-bridge hexa-substituted Dawson-type-based layer $[Ni_6(\mu_3\text{-}OH)_3$-$(dap)_2(en)(H_2O)\{OOC(CH_2)_2COO\}_{0.5}(CH_3COO)(P_2W_{15}O_{56})]$ (Figure 4g) [23,24]. The AP in **3** is the longest aliphatic dicarboxylic acid being incorporated in POMs family. Moreover, it differs from those 1D chains with a TM–O=W linkage and 1D POMCOCs featuring strict chains [7,29]; the 1D helical chains in **3** are the first 1D POMCOC with helical features.

Since the hexa-$Ni^{II}$ cluster of **1**–**3** is similar to those in the reported hexa-Ni- substituted TMSPs, we compared their bond lengths and bond angles to speculate the magnitude properties of the title compounds. As shown in Table S1 (Supplementary Materials), the Ni–O bond lengths and Ni–O–Ni bond angles of **1**–**3** are in the ranges of 1.915–2.295 Å and 90.9–114.2°, respectively. According to the previous research [4,7,31,38,39], when the Ni–O–Ni bond angles are in the range of 90–104°, ferromagnetic exchange interactions are dominant. When Ni–O–Ni bond angles are larger than 104°, anti-ferromagnetic exchange interactions may exist. When ferromagnetic and antiferromagnetic behaviors coexist, the overall magnetic behaviors are determined by which one is dominant. Normally, most of the Ni–O–Ni bond angles in the hexa-$Ni^{II}$ cluster are in the ferromagnetic dominant ranges when ferromagnetic and antiferromagnetic coupling coexistences appear. Ferromagnetic exchange behaviors are expected for hexa-$Ni^{II}$ clusters, which have been proved by the

measurements in our previous research [4,7,31,38,39]. In **1**, since all the Ni–O–Ni bond angles are in the range of 92.5–102.1°, ferromagnetic exchange behaviors are expected. In **2** and **3**, the Ni–O–Ni bond angles are in the range of 90.9–106.8° and 91.6–114.2°, respectively, indicating the coexistences of ferromagnetic and antiferromagnetic couplings. There are only 1 and 2 Ni–O–Ni bond angles larger than 104°, indicating that the ferromagnetic exchange behaviors are dominant in **2** and **3**, similar to those reported in hexa-$Ni^{II}$-substituted TMSPs.

### *3.5. Powder XRD Patterns*

As shown in Figure S3 (Supplementary Materials), the experimental PXRD patterns of **1**–**3** were all consistent with the simulated patterns obtained from single-crystal data, which confirm the purities of the samples. The differences in the intensities were attributable to the preferred orientations.

### *3.6. IR Spectra*

As shown in Figure S4 (Supplementary Materials), the IR spectra of **1**–**3** show a series of similar absorption bands ranging from 4000–400 $cm^{-1}$. The wide absorption bands from 3528 to 3134 $cm^{-1}$ are assigned to the stretching vibrations of the –OH, $–CH_2$, and $–NH_2$ groups. The sharp absorption peaks from 3005 to 2817 $cm^{-1}$ are the stretching vibrations of the $–CH_2$ and $–NH_2$ groups. The peaks ranging from 1652–1363 $cm^{-1}$ are the characteristic peaks of the bending vibrations of $–NH_2$ and $–CH_2$ groups in **1**–**3** and the carboxylate groups of the carboxylate ligands in **2**–**3**. Four intense characteristic peaks of $v$(P–O), $v$(W–$O_t$), $v$(W–$O_b$), and $v$(W–$O_c$) of the Keggin-fragments are observed at 1039, 941, 842, 796, and 716 $cm^{-1}$ for **1**, 1033, 935, 841, 796, and 715 $cm^{-1}$ for **2**, and 1037, 943, 848, 796, and 710 $cm^{-1}$ for **3**, respectively.

### *3.7. UV-Vis Absorption Spectra*

In order to investigate the optical properties of the title compounds, UV-Vis absorption and optical diffuse reflectance spectra of **1**–**3** were obtained in the wavelength range of 190–800 nm. As shown in Figure S5 (Supplementary Materials), the optical band gaps of **1**–**3** are 2.60, 2.59, and 2.56 eV, respectively, which are comparable to other $Ni_6$-substitute POMs, including $[Ni_6(\mu_3\text{-}OH)_3(en)_2(dien)(H_2O)_5(B\text{-}\alpha\text{-}PW_9O_{34})]\cdot 3H_2O$ (2.42 eV), $[Ni_6(\mu_3\text{-}OH)_3(dap)_2(py)_6\text{-}(H_2O)(B\text{-}\alpha\text{-}PW_9O_{34})]\cdot H_2O$ (2.37 eV), and $[Ni(en)_2][Ni_6(\mu_3\text{-}OH)_3(en)_3(1,3\text{-}bdc)(H_2O)_2(B\text{-}\alpha\text{-}PW_9O_{34})]\cdot 9H_2O$ (2.53 eV) [20,29]. It was found that the band gaps of **1**–**3** are in the order of **3** < **2** < **1**, which conforms to the band gaps of the compounds decreasing with the increasing dimensionality or complexity of the structures, as proposed by Kanatzidis and Papavassiliou [40].

## 4. Conclusions

In summary, three new TMSPs containing $\{Ni_6PW_9\}$ units were designed and synthesized from monomers to 1D POMCOC under hydrothermal conditions. **1** is a monomer with DACH molecules decorating the $Ni_6$ cluster. In order to construct POMCOF on the basis of **1**, the rigid aromatic MIP ligand was first incorporated and the anionic monomeric POM **2** was obtained. HMIP still acts as a decorating group on the $Ni_6$ cluster but fails to bridge adjacent $\{Ni_6PW_9\}$ units. By analyzing the orientations and steric hindrance between adjacent $\{Ni_6PW_9\}$ units of **2**, the aliphatic AP ligand was purposely chosen to replace HMIP on the base of **2**, which resulted in the formation of **3**, a new 1D POMCOC with novel helical chain. Owing to the good flexibility of the AP linker, **3** represents the first 1D POMCOC with a helical chain. This work is an example of our continued work of constructing POMCOFs with hexa-$Ni^{II}$ substituted TMSP SBUs. The successfully designed syntheses from **1** to **3** provide us with a new strategy of using chainlike dicarboxylate acid as a linker to make POMCOFs, which may lead to some intriguing structures that cannot be found with rigid aromatic linkers. Further works with this strategy are in progress.

**Supplementary Materials:** The following supporting information can be downloaded at: https://www.mdpi.com/article/10.3390/molecules27134295/s1, Table S1: Comparisons of the bond lengths and bond angles in $Ni_6$-subsi- tuted TMSPs; Figure S1: Asymmetric units of **1**–**3**; Figure S2: $[Ni(DACH)_2]^{2+}$ complex in **2** and **3**; Figure S3: PXRD of **1**–**3**. Figure S4: IR spectra of **1**–**3**; Figure S5: UV-Vis spectra of **1**–**3**; Figure S6: TG curves of **1**–**3**. [41–43] are cited in the Supplementary Materials.

**Author Contributions:** Conceptualization, C.-A.C.; methodology, C.-A.C. and Y.L.; formal analysis, C.-A.C. and Y.L.; data curation, Y.L.; writing—original draft, preparation, C.-A.C.; writing—reviewing and editing, supervision, and funding acquisition: G.-Y.Y. All authors have read and agreed to the published version of the manuscript.

**Funding:** This research was funded by the National Natural Science Foundation of China, grant numbers 21831001, 21571016, 91122028 and 20725101.

**Institutional Review Board Statement:** Not applicable.

**Informed Consent Statement:** Not applicable.

**Data Availability Statement:** Not applicable.

**Conflicts of Interest:** The authors declare no conflict of interest.

**Sample Availability:** Samples of the compounds are available from the authors.

## References

1. Zheng, S.-T.; Yang, G.-Y. Recent advances in paramagnetic-TM-substituted polyoxometalates (TM = Mn, Fe, Co, Ni, Cu). *Chem. Soc. Rev.* **2012**, *41*, 7623–7646. [CrossRef] [PubMed]
2. Wang, S.-S.; Yang, G.-Y. Recent advances in polyoxometalate-catalyzed reactions. *Chem. Rev.* **2015**, *115*, 4893–4962. [CrossRef] [PubMed]
3. Liu, J.X.; Zhang, X.B.; Li, Y.L.; Huang, S.L.; Yang, G.Y. Polyoxometalate functionalized architectures. *Coord. Chem. Rev.* **2020**, *414*, 213260–213275. [CrossRef]
4. Zheng, S.-T.; Yuan, D.-Q.; Jia, H.-P.; Zhang, J.; Yang, G.-Y. Combination between lacunary polyoxometalates and high-nuclear transition metal clusters under hydrothermal conditions: I. from isolated cluster to 1-D chain. *Chem. Commun.* **2007**, *18*, 1858–1860. [CrossRef]
5. Pichon, C.; Mialane, P.; Dolbecq, A.; Marrot, J.; Rovière, E.; Bassil, B.S.; Kortz, U.; Keita, B.; Nadjo, L.; Sécheresse, F. Octa- and Nonanuclear nickel(II) polyoxometalate clusters: Synthesis and electrochemical and magnetic characterizations. *Inorg. Chem.* **2008**, *47*, 11120–11128. [CrossRef]
6. Ibrahim, M.; Xiang, Y.; Bassil, B.S.; Lan, Y.H.; Powell, A.K.; Oliveira, P.D.; Keita, B.; Kortz, U. Synthesis, magnetism, and electro -chemistry of the $Ni_{14}$- and $Ni_5$-Containing heteropolytungstates $[Ni_{14}(OH)_6(H_2O)_{10}(HPO_4)_4(P_2W_{15}O_{56})_4]^{34-}$ and $[Ni_5(OH)_4(H_2O)_4$- (β-$GeW_9O_{34}$)(β-$GeW_8O_{30}$(OH))$]^{13-}$. *Inorg. Chem.* **2013**, *52*, 8399–8408. [CrossRef]
7. Zheng, S.T.; Zhang, J.; Yang, G.-Y. Designed synthesis of POM–organic frameworks from $\{Ni_6PW_9\}$ building blocks under hydrothermal conditions. *Angew. Chem. Int. Ed.* **2008**, *47*, 3909–3913. [CrossRef]
8. Li, X.-X.; Wang, Y.-X.; Wang, R.-H.; Cui, C.-Y.; Tian, C.-B.; Yang, G.-Y. Designed assembly of heterometallic cluster organic frameworks based on Anderson-type polyoxometalate clusters. *Angew. Chem. Int. Ed.* **2016**, *55*, 6462–6466. [CrossRef]
9. Li, X.-X.; Zhao, D.; Zheng, S.-T. Recent advances in POM-organic frameworks and POM-organic polyhedra. *Coord. Chem. Rev.* **2019**, *397*, 220–240. [CrossRef]
10. Schubert, U. Cluster-based inorganic–organic hybrid materials. *Chem. Soc. Rev.* **2011**, *40*, 575–582. [CrossRef]
11. Fang, W.-H.; Yang, G.-Y. Induced aggregation and synergistic coordination strategy in cluster organic architectures. *Acc. Chem. Res.* **2018**, *51*, 2888–2896. [CrossRef] [PubMed]
12. Lin, L.-D.; Zhao, D.; Li, X.-X.; Zheng, S.-T. Recent advances in zeolite-like cluster organic frameworks. *Chem. Eur. J.* **2019**, *25*, 442–453. [CrossRef] [PubMed]
13. Dolbecq, A.; Mellot-Draznieks, C.; Mialane, P.; Marrot, J.; Férey, G.; Sécheresse, F. Hybrid 2D and 3D frameworks based on ϵ-Keggin polyoxometallates: Experiment and simulation. *Eur. J. Inorg. Chem.* **2005**, *2005*, 3009–3018. [CrossRef]
14. Wang, Y.-R.; Huang, Q.; He, C.-T.; Chen, Y.-F.; Liu, J.; Shen, F.-C.; Lan, Y.-Q. Oriented electron transmission in polyoxometalate-metalloporphyrin organic framework for highly selective electroreduction of $CO_2$. *Nat. Commun.* **2018**, *9*, 4466–4474. [CrossRef] [PubMed]
15. Li, X.-X.; Zhang, L.-J.; Cui, C.-Y.; Wang, R.-H.; Yang, G.-Y. Designed construction of cluster organic frameworks from Lindqvist-type polyoxovanadate cluster. *Inorg. Chem.* **2018**, *57*, 10323–10330. [CrossRef]
16. Han, J.-W.; Hill, C.-L. A Coordination network that catalyzes $O_2$-based oxidations. *J. Am. Chem. Soc.* **2007**, *129*, 15094–15095. [CrossRef]

17. Marleny Rodriguez-Albelo, L.; Ruiz-Salvador, A.R.; Sampieri, A.; Lewis, D.W.; Gómez, A.; Nohra, B.; Mialane, P.; Marrot, J.; Sécheresse, F.; Mellot-Draznieks, C.; et al. Zeolitic polyoxometalate-based metal−organic frameworks (Z-POMOFs): Computational evaluation of hypothetical polymorphs and the successful targeted synthesis of the redox-active Z-POMOF. *J. Am. Chem. Soc.* **2009**, *131*, 16078–16087. [CrossRef]
18. Wang, Y.-Y.; Zhang, M.; Li, S.-L.; Zhang, S.-R.; Xie, W.; Qin, J.-S.; Su, Z.-M.; Lan, Y.-Q. Diamondoid-structured polymolybdate -based metal–organic frameworks as high-capacity anodes for lithium-ion batteries. *Chem. Commun.* **2017**, *53*, 5204–5207. [CrossRef]
19. Cheng, W.; Shen, F.-C.; Xue, Y.-S.; Luo, X.; Fang, M.; Lan, Y.-Q.; Xu, Y. A pair of rare three-dimensional chiral polyoxometalate-based metal–organic framework enantiomers featuring superior performance as the anode of lithium-ion battery. *ACS Appl. Energy Mater.* **2018**, *1*, 4931–4938. [CrossRef]
20. Zhang, Z.; Wang, Y.-L.; Li, H.-L.; Sun, K.-N.; Yang, G.-Y. Syntheses, structures and properties of three organic–inorganic hybrid polyoxotungstates constructed from $\{Ni_6PW_9\}$ building blocks: From isolated clusters to 2-D layers. *CrystEngComm* **2019**, *21*, 2641–2647. [CrossRef]
21. Li, X.-X.; Shen, F.-C.; Liu, J.; Li, S.-L.; Dong, L.-Z.; Fu, Q.; Su, Z.-M.; Lan, Y.-Q. A highly stable polyoxometalate-based metal–organic framework with an ABW zeolite-like structure. *Chem. Commun.* **2017**, *53*, 10054–10057. [CrossRef] [PubMed]
22. Wang, X.-L.; Liu, X.-J.; Tian, A.-X.; Ying, J.; Lin, H.-Y.; Liu, G.-C.; Gao, Q. A novel 2D→3D $\{Co_6PW_9\}$-based framework extended by semi-rigid bis(triazole) ligand. *Dalton Trans.* **2012**, *41*, 9587–9589. [CrossRef] [PubMed]
23. Rousseau, G.; Oms, O.; Dolbecq, A.; Marrot, J.; Mialane, P. Route for the elaboration of functionalized hybrid 3d-substituted trivacant Keggin anions. *Inorg. Chem.* **2011**, *50*, 7376–7378. [CrossRef] [PubMed]
24. Wang, X.-Q.; Liu, S.-X.; Liu, Y.-W.; He, D.-F.; Li, N.; Miao, J.; Ji, Y.-J.; Yang, G.-Y. Planar $\{Ni_6\}$ cluster-containing polyoxometalate-based inorganic–organic hybrid compound and its extended structure. *Inorg. Chem.* **2014**, *53*, 13130–13135. [CrossRef]
25. Ginsberg, A.-P. *Inorganic Syntheses*; John Wiley & Sons: New York, NY, USA, 1990; p. 108.
26. Sheldrick, G.M. A short history of SHELX. *Acta Crystallogr. Sect. A Found. Crystallogr.* **2008**, *64*, 112–122. [CrossRef]
27. Brown, I.D.; Altermatt, D. Bond-valence parameters obtained from a systematic analysis of the inorganic crystal structure database. *Acta Crystallogr. Sect. B* **1985**, *41*, 244–247. [CrossRef]
28. Kariem, M.; Kumar, M.; Yawer, M.; Sheikh, H.M. Solvothermal synthesis and structure of coordination polymers of Nd(III) and Dy(III) with rigid isophthalic acid derivatives and flexible adipic acid. *J. Mol. Struct.* **2017**, *1150*, 438–446. [CrossRef]
29. Sun, J.J.; Wang, Y.L.; Yang, G.-Y. Two new hexa-Ni-substituted polyoxometalates in the form of an isolated cluster and 1-D chain: Syntheses, structures, and properties. *CrystEngComm* **2020**, *22*, 8387–8393. [CrossRef]
30. Sun, J.-J.; Wang, W.-D.; Li, X.-Y.; Yang, B.-F.; Yang, G.-Y. $\{Cu_8\}$ cluster-sandwiched polyoxotungstates and their polymers: Syntheses, structures, and properties. *Inorg. Chem.* **2021**, *60*, 10459–10467. [CrossRef]
31. Zhao, J.-W.; Jia, H.-P.; Zhang, J.; Zheng, S.-T.; Yang, G.-Y. A combination of lacunary polyoxometalates and high-nuclear transition-metal clusters under hydrothermal conditions. Part II: From double cluster, dimer, and tetramer to three-dimensional frameworks. *Chem. Eur. J.* **2007**, *13*, 10030–10045. [CrossRef]
32. Li, B.; Zhao, J.-W.; Zheng, S.-T.; Yang, G.-Y. Combination chemistry of hexa-copper-substituted polyoxometalates driven by the $Cu^{II}$-polyhedra distortion: From tetramer, 1D chain to 3D framework. *Inorg. Chem.* **2009**, *48*, 8294–8303. [CrossRef] [PubMed]
33. Zhao, J.-W.; Wang, C.-M.; Zhang, J.; Zheng, S.-T.; Yang, G.-Y. Combination of lacunary polyoxometalates and high-nuclear transition metal clusters under hydrothermal conditions: IX. A series of novel polyoxotungstates sandwiched by octa-copper clusters. *Chem. Eur. J.* **2008**, *14*, 9223–9239. [CrossRef] [PubMed]
34. Zhao, J.-W.; Li, B.; Zheng, S.-T.; Yang, G.-Y. Two-dimensional extended (4,4)-topological network constructed from tetra-$Ni^{II}$-substituted sandwich-type Keggin polyoxometalate building blocks and $Ni^{II}$-organic cation bridges. *Cryst. Growth Des.* **2007**, *7*, 2658–2664. [CrossRef]
35. Li, Y.-X.; Zhang, Z.; Yang, B.-F.; Li, X.-X.; Zhang, Q.; Yang, G.-Y. A two-dimensional (4,4)-network built by tetra-Ni- substituted sandwich-type Keggin polyoxoanions linked by different Ni-organoamine complexes. *Inorg. Chem. Commun.* **2017**, *75*, 12–15. [CrossRef]
36. Zheng, S.-T.; Zhang, J.; Clemente-Juan, J.M.; Yuan, D.-Q.; Yang, G.-Y. Poly(polyoxotungstate)s with 20 nickel centers: From nanoclusters to one-dimensional chains. *Angew. Chem. Int. Ed.* **2009**, *48*, 7176–7179. [CrossRef]
37. Li, X.-X.; Fang, W.-H.; Zhao, J.-W.; Yang, G.-Y. The first 3-connected $SrSi_2$-type 3D chiral framework constructed from $\{Ni_6PW_9\}$ building units. *Chem. Eur. J.* **2015**, *21*, 2315–2318. [CrossRef]
38. Zheng, S.-T.; Zhang, J.; Li, X.-X.; Fang, W.-H.; Yang, G.-Y. Cubic polyoxometalate—Organic molecular cage. *J. Am. Chem. Soc.* **2010**, *132*, 15102–15103. [CrossRef]
39. Huang, L.; Zhang, J.; Cheng, L.; Yang, G.-Y. Poly(polyoxometalate)s assembled by $\{Ni_6PW_9\}$ units: From ring-shaped $Ni_{24}$-tetramers to rod-shaped $Ni_{40}$-octamers. *Chem. Commun.* **2012**, *48*, 9658–9660. [CrossRef]
40. Axtell, E.A.; Park, Y.; Chondroudis, K.; Kanatzidis, M.G. Incorporation of $A_2Q$ into HgQ and dimensional reduction to $A_2Hg_3Q_4$ and $A_2Hg_6Q_7$ (A = K, Rb, Cs; Q = S, Se). Access of Li Ions in $A_2Hg_6Q_7$ through topotactic ion-exchange. *J. Am. Chem. Soc.* **1998**, *120*, 124–136. [CrossRef]

41. Müller, A.; Beckmann, E.; Bögge, H.; Schmidtmann, M.; Dress, A. Inorganic Chemistry Goes Protein Size: A Mo368 Nano-Hedgehog Initiating Nanochemistry by Symmetry Breaking. *Angew. Chem. Int. Ed.* **2002**, *41*, 1162–1167. [CrossRef]
42. Mialane, P.; Dolbecq, A.; Marrot, J.; Rivieère, E.; Seécheresse, F. A Supramolecular Tetradecanuclear Copper(II) Polyoxotungstate. *Angew. Chem. Int. Ed.* **2003**, *42*, 3523–3526. [CrossRef] [PubMed]
43. Huang, L.; Wang, S.-S.; Zhao, J.-W.; Cheng, L.; Yang, G.-Y. Synergistic Combination of Multi-$Zr^{IV}$ Cations and Lacunary Keggin Germanotungstates Leading to a Gigantic $Zr_{24}$-Cluster-Substituted Polyoxometalate. *J. Am. Chem. Soc.* **2014**, *136*, 7637–7642. [CrossRef] [PubMed]